

Fatigue evaluation and enhanced shear strain measurements of bonded composite joints

T. Löbel, H. Sonnenberg, D. Holzhüter, C. Hühne

DLR, German Aerospace Center
Lilienthalplatz 7, 38108 Braunschweig, Germany
thomas.loebel@dlr.de

Keywords: Adhesive Bonding; Digital image correlation (DIC); Fatigue; Crack growth.

Summary: *In this study, the crack growth behavior and shear stress distribution under typical loading conditions is studied for a composite bonded joint. A novel approach of strain measurement is presented by using a high-resolution digital image correlation system (DIC) which allows detailed investigations of the shear strain distribution within the bondline. By testing 7 different load levels with 3 specimens each in fatigue the crack growth rates, the crack growth threshold and the Paris Law correlation are obtained for an aerospace epoxy adhesive.*

1. INTRODUCTION

1.1 Today's usage and limitations of bonded composite joint for aircraft applications

Implementing more CFRP load-bearing parts to achieve competitive lightweight structures demands efficient solutions in terms of joining technology. With bolting on the one hand and adhesive bonding on the other, there are two major joining techniques available for thermoset composites which are the majority of composites used for aeronautical applications. From a mechanical perspective, adhesive bonding is the favorable joining technique for several reasons. Adhesive bonds lead to weight reduction, offer a more uniform load distribution, are capable of joining thin-walled parts and minimize material weakening. The presence of fasteners has a noticeable impact on the part design and could even be a key dimensioning factor and thereby hamper the full lightweight potentials of composites [1]. Therefore, the development of adhesive bonds being capable for certification is of high interest.

For civil aircraft, bonding of composites is well-established for various secondary joints. Airbus' A380 features bonded joints for instance in the rear pressure bulkhead, the ailerons, the vertical tail plane and the radome [3] as shown in Fig. 1. For the latest aircraft of the Airbus family (Airbus A350XWB), a large share of stiffeners are (composite to composite) bonded joints leading to an overall bondline length of about 5 km per aircraft [2].

However, due to certification requirements [4, 5] the implementation of bonded joints in aircraft composite structures is still limited to secondary joints or combined with so called "chicken rivets" if used in primary joints. Those additional fasteners have to be capable to carry relevant loads in case of a global failure of the bondline [2]. Design benefits that come along with adhesive bonding don't come into effect, since fastening elements must be taken into account for part design. Thus, the potential of adhesive bonding is not used to its full extent.

Besides manufacturing uncertainties (e.g. surface treatment, curing cycle and humidity), aging and fatigue life of bonded composite joints is still challenging to predict and influenced by many factors (e.g. load level, strain rate and environmental conditions) [6, 7, 8]. Furthermore, in-service damages (e.g. impact events) could hardly be avoided and may lead to a noticeable decrease of the joint's strength [6, 9]. Eventually, all those factors led in some cases to significant scatter in the performance of bonded composite joints in the past with some working well and some failing after short time in service [10]. Those experiences have caused a distrust towards adhesive bonding as joining technology.

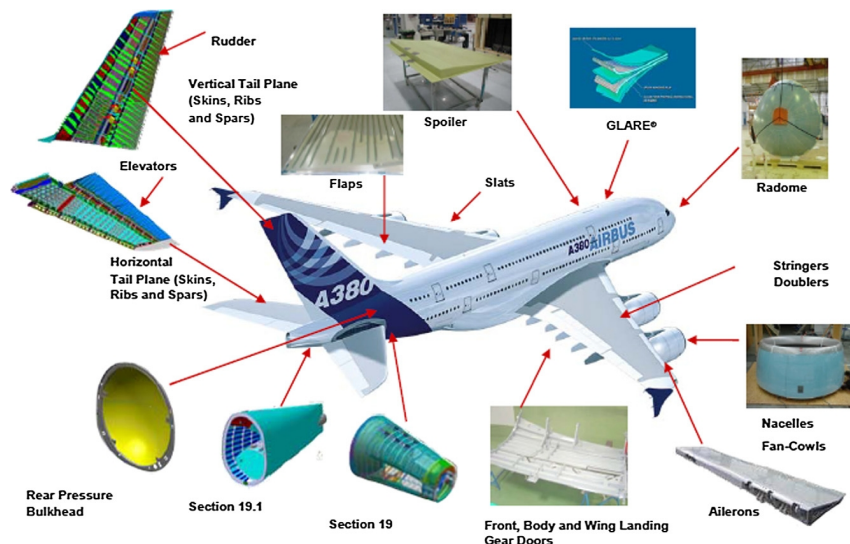


Figure 1. Usage of adhesive bonding in the Airbus A380 [3]

1.2 Framework for the experimental investigations in this study

As discussed above, the potential existence of local weak bonds due to flaws or deviations during manufacturing or due to in-service damage events must be taken into account for bonded joints. Stress concentrations at disbond edges may lead to growing cracks under fatigue loading conditions. According to the regulations [4, 5], one promising way to achieve airworthiness of bonded CFRP joints is the establishment of disbond-constraining design features. Based on this situation, finding, designing and evaluating possible disbond stopping design features

is the overall goal of the European Project BOPACS¹. To evaluate such features, the crack growth behavior and the stress distribution within the bondline under typical loading conditions is studied.

2. SPECIMEN DESIGN AND TEST DEFINITION

2.1 General Considerations

The *Crack Lap Shear* (CLS) specimen as shown in Fig.2 is chosen for all tests. The configuration is predominantly loaded in shear and especially representative for long low loaded overlap joints (e.g. stringer to skin configurations). CLS tests are often used to obtain fracture toughness data. The test configuration allows defined crack propagation. Various studies (e.g. [11]) show that the mixed mode ratio (peel to shear) within the bondline is almost constant for different crack length. Analytical closed form solutions [12] also indicate that the fracture toughness is independent of the crack length. Thus, the CLS specimen would also be applicable for investigations of crack-stopping design features.

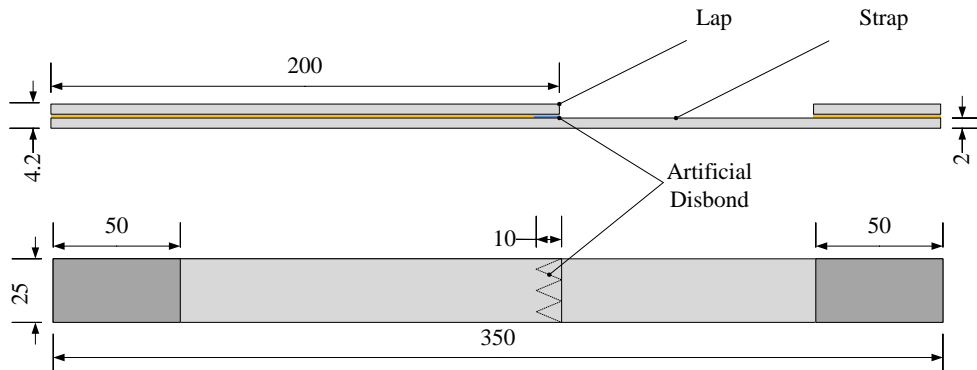


Figure 2. CLS geometry (all length in mm)

A zigzag shaped release film is used to introduce the crack in the adhesive at the edge from strap to lap. Thereby, crack initiation is believed to be more even and thus predictable. A rather long lap section is chosen to avoid clamping effects on the crack growth for about 100 mm crack length. Besides, the long overlap allows the implementation of crack-constraining design features in subsequent studies. An additional tab is bonded at the strap's end (clamping area) to avoid an eccentric test setup. No additional tabs are used on the opposite (lap) side.

¹Boltless assembling of Primary Aerospace Composite Structures

2.2 Static Tests

Static tests are carried out displacement driven with 2 mm/min at room temperature. The undisturbed tensile strength of the CLS configuration is determined by testing 9 specimens without any artificial disbond. The specimen's strain is determined by the use of strain gauges on the strap and lap.

2.3 Preliminary dynamic-mechanical analysis (DMA)

Toughened adhesives show a strain-rate dependency due to visco-elastic effects [9]. Since the strain-rate dependency might effect the test results, a suitable test frequency for fatigue tests needs to be determined that minimizes testing time and also avoids undesired strain-rate hardening. Therefore, dynamic-mechanical analysis (DMA) is used to determine the strain-rate dependency of the adhesive's elastic modulus.

A rectangular bar of pure adhesive (60 mm x 5 mm x 2 mm) is tested in three point bending according to ASTM D5023-01. The modulus (both, elastic and loss) is determined at isothermal conditions (20° C) as a function of frequency.

Table 1. DMA results: strain-rate dependency of elastic modulus

test frequency [Hz]	1	2	3	4	5	6	7	8	9	10
relative increase of modulus [%]	0	0.61	0.98	1.27	1.43	1.72	1.84	1.88	2.00	2.25

As indicated in Table 1, a slight stiffness increase is measured for frequencies between 1 Hz and 10 Hz. However, the influence is rather small (less than 2.5 %). Therefore, the test frequency for fatigue tests is set to 8 Hz in agreement with project partners. A thermal influence due to frictional heat is not expected.

2.4 Fatigue Tests

As for the static load case, all tests are carried out at room temperature. The tests are conducted at 7 different load levels (see Table 2) with 3 specimens for each load level in order to get a profound data base for fatigue evaluation. The maximum loads (F_{max}) are chosen as a value of strain in the middle of the strap between the overlap and the clamping region. Although all tests are executed load driven, a strain correlation is made based on measurements that are executed by the use of strain gauges. The load levels are also given in Table 2 as share of the ultimate static strength ($F_{ultimate}$) that is determined beforehand in static tests.

All tests are carried out with a constant amplitude at 8 Hz sinusoidal with a load ratio R of 0.1 (tensile-tensile loading) using a servo-hydraulic test machine. The test is terminated either after

10^6 load cycles or after the crack length equals 90 mm. Thus, the maximum testing time per specimen amounts to approximately 35 hours.

Table 2. Chosen load levels for fatigue tests

F_{max} [kN]	5.16	7.69	9.28	10.86	12.43	15.6
$F_{max}/F_{ultimate}$ [%]	19	29	35	40	46	58
strap strain [$\mu m/m$]	1700	2500	3000	3500	4000	5000

3. MATERIALS AND MANUFACTURING

Specimens are manufactured using Hexply 8552/IM7 unidirectional prepreg material. The composite plates consist of 16 plies $[0/+45/90/-45/0/+45/90/-45]_s$ leading to a plate thickness of 2 mm. The 0° surface plies in longitudinal direction are chosen to minimize undesired delamination failure close to the bondline while testing as described by Baker [1] and Lin et al. [13]. A PTFE release film between the plate's surface and the steel tooling ensures a constant overall surface finish. Curing of the prepreg system (180°C , 7 bar autoclave cycle) is done in accordance with the data sheet specifications.

After cleaning with isopropanol, atmospheric plasma is used for surface treatment of bonding surfaces (Plasmatreat generator FG5001). The process parameters were obtained in previous studies for optimized surface activation.

Loctite EA 9695 0.05 PSF K as common high strength film adhesive for aerospace applications is used as adhesive system. The one-component epoxy film has an average thickness of 0.15 mm after curing. As for the prepreg material, curing is done in an autoclave cycle (180°C , 3.5 bar) to ensure high quality bonding. Afterwards, all plates are trimmed and cut to the final specimen dimensions as specified in Fig. 2.

4. MEASUREMENT INSTRUMENTATION

4.1 Digital Image Correlation

The digital image correlation (DIC) system Aramis by Gom is used in static tests allowing a contact-free measurement of the strain field by examination of the specimen's edge (side view). The investigation area is divided into a field of facettes which are small rectangular fractions of the surface. All displacement and deformation calculations are based on the facette form and position in comparison to a (initial) reference stage. To distinguish between two neighboring facettes, a very fine and high contrast surface structure is needed. A very fine and random surface pattern is obtained by the use of 2 paint-sprays (black and white).

For detailed examinations of the bondline, a field of view of 10 mm by 7.5 mm is chosen leading to a very fine field of facettes which one facette having the size of 0.017 mm by 0.017 mm. Due to the high-contrast surface pattern, almost 10 facettes are obtained in the bondline thickness of 0.15 mm. Thus, deformations of the adhesive itself are directly measured at the overlap edge from strap to lap where high deformations and stresses occur (see Fig. 3).

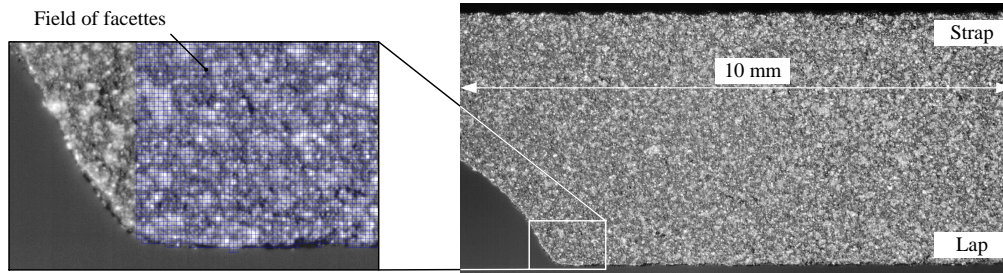


Figure 3. Aramis setup: left - field of facettes; right- overall field of view with fine paint-spray surface pattern

4.2 Crack growth measurement

It is mandatory to measure the developing crack in its length for fatigue investigations. Preliminary trials of back face strain measurements by the use of strain gauges at distinct positions on the lap turned out to be not accurate enough. Therefore, two microscopes, one for each side, are used. To obtain a crack opening of high contrast, both edges are painted in white by the use of paint-spray. A mm-scale is manually plotted on the surface for crack length determination. Additionally, one microscope is mounted to an electric travel measurement system allowing a crack length reading with the accuracy of ± 0.01 mm. The test setup is shown in Fig. 4.

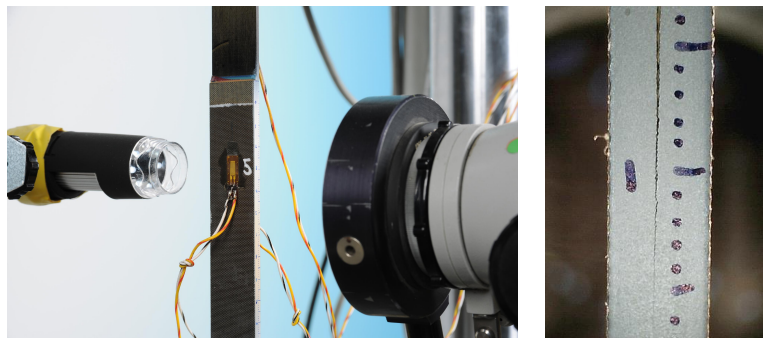


Figure 4. Left: fatigue test setup with two microscopes for crack length measurement, right: crack opening during test

The crack measurement is done every 28 800 load cycles. For high load levels ($4000 \mu m/m$ and $5000 \mu m/m$) the measurement is done more frequently.

5. RESULTS

5.1 Static tests

The static tensile strength of the CLS configuration is determined to 26.83 kN with a standard deviation (SD) of 3.6 %. A thin layered cohesive failure with a minor share of delamination (first ply) is observed as fracture pattern which is typical for this test configuration (see Fig. 5).

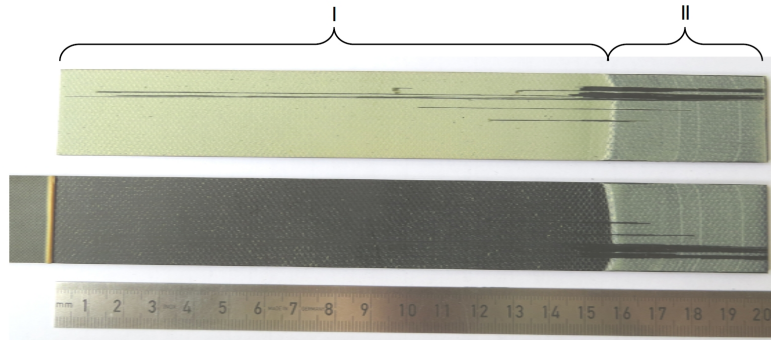


Figure 5. I-fracture surface after static test; II - fracture pattern within clamping area created manually after testing

The Aramis measurements allow the determination of the shear angle as function of the applied load as well as function of the position along the bondline. However, since the directly measured shear angle values within the bondline show some scatter, it is determined indirectly by comparing the displacement along two lines (one on each adherend) with one being close to the upper bondline edge (δ_1) and the other close to the lower bondline edge (δ_2). As the distance between both lines is known (l), the relative displacement of points on the line can be used to determine the shear angle (γ) of the bondline by straight forward calculations as shown in equation (1). The displacement measurements show less scatter and thereby allow a more accurate calculation of the shear angle.

$$\tan(\gamma) \approx \gamma = \frac{\Delta\delta}{l} \quad (1)$$

As expected, maximum shear appears at the overlap edge between strap to lap (Figure 6). The shear angle and the shear stress of the bond respectively, progressively decrease with increasing distance from the overlap edge. Failure initiates when the adhesive strength is locally exceeded.

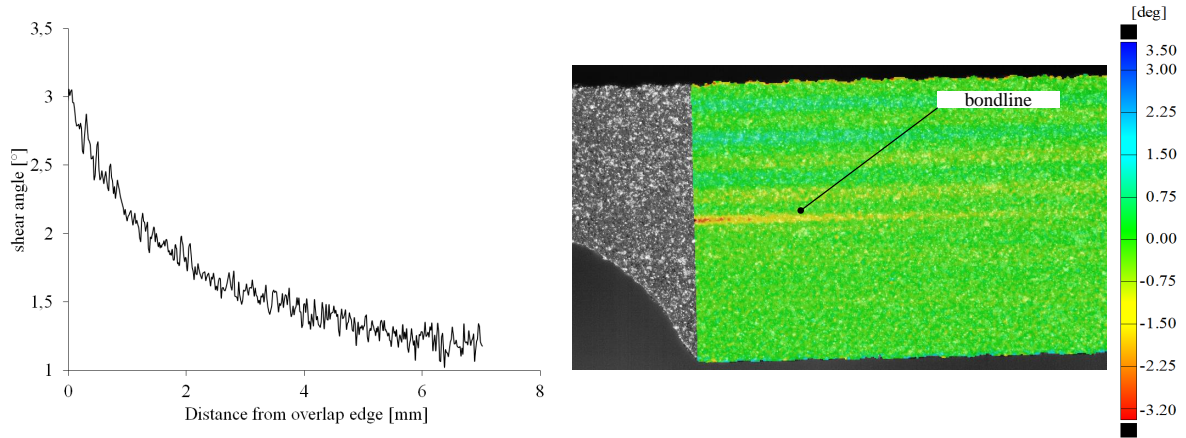


Figure 6. Measured shear angle along the bondline at 9.79 kN tensile load

The calculations of the maximum shear angle within the bondline are summarized for the load levels of interest for fatigue in Table 3.

5.2 Fatigue tests

The comparison of the crack length readings for both edges show only minor deviations of the crack length (over the specimen's width) of ± 2 mm. Thus, it can be concluded that the crack propagates almost perpendicular to the direction of loading.

The derived crack length as function of the cycle numbers is shown in Fig. 7 for the 3 most relevant load levels. Those are considered to be most relevant, since the value of $3000 \mu\text{m/m}$ global strain is often referred as the maximum limit load strain for aeronautical applications which represents the relevant service load.

As shown in Fig. 7, deviations occur for both, crack initiation and crack growth rate. However, similar load levels lead to comparable results and only minor deviations occur.

A thin layered cohesive fracture pattern is observed for all specimen without any delamination.

It shall be emphasized, that for a low load level of $2500 \mu\text{m/m}$ global strain crack growth initiates not until about 2×10^5 cycles even with the teflon release film as starter crack being implemented.

Furthermore, the lowest load level of $1700 \mu\text{m/m}$ global strain which equals about 19 % of the static fracture load, does not lead to any crack growth beyond the zigzag release film for the 10^6 cycles tested as shown in Fig. 8. By measuring the overall fracture that occurs during fatigue (sum of length I, II and III, Fig. 8), the crack growth threshold value could be estimated by correlating the fractured width with the overall specimen's width. The sum of the fractured

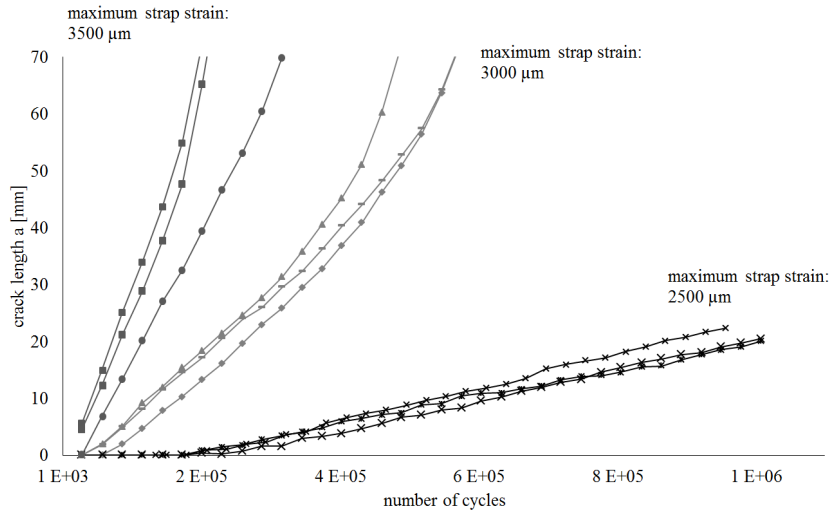


Figure 7. Measured crack length for different (low) load levels

area amounts to 67 % of the overall width. Thus, the threshold for fatigue crack growth (S_t) is assumed as follows:

$$S_t = \frac{1700 \mu\text{m}/\text{m}}{0.67} = 2537 \mu\text{m}/\text{m} \quad (2)$$

The corresponding maximum force for S_t amounts to 7.69 kN.

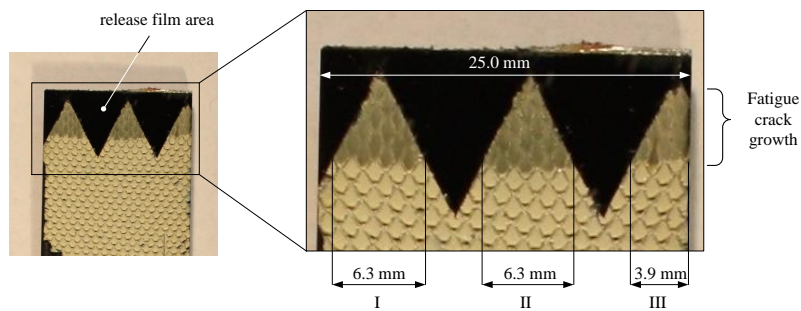


Figure 8. Fracture pattern for specimen tested at $1700 \mu\text{m}/\text{m}$ global maximum strain

A summary of the crack growth rate da/dN is given as a function of the strain energy release rate (ERR) ΔG in Fig. 9. This relation (*Paris law*) between the ERR and the sub-critical crack growth rate can be described as:

$$\frac{da}{dN} = C \cdot \Delta G^m \quad (3)$$

Whereas the material constants for the adhesive C and m amounts to $1.425 \cdot 10^{-10}$ and 3.577. The ERR is derived analytically as shown by Johnson [11] and Wang [12]:

$$\Delta G = \frac{\partial U_E}{\partial A} = \frac{(\Delta P)^2}{2b(EA)_2} \left[1 - \frac{(EA)_2}{(EA)_0} \right] \quad (4)$$

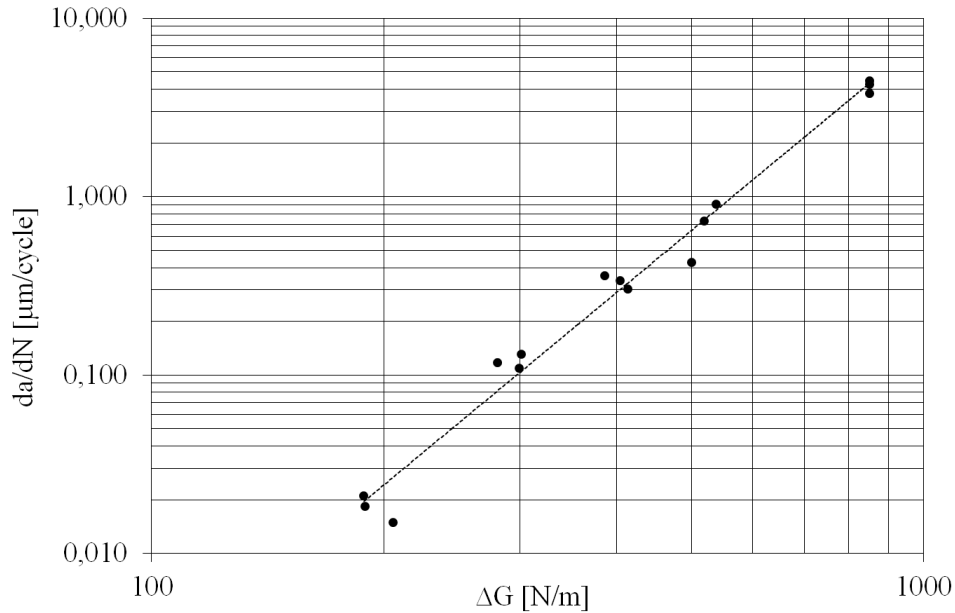


Figure 9. Crack growth rate da/dN for the load levels tested as function of the energy release rate ΔG

In this equation P is the applied load, b is the specimen width, $(EA)_2$ is the tensile rigidity of the strap and $(EA)_0$ the total tensile rigidity. By assuming that the total stiffness of strap and lap approximately equals the strap's stiffness and the sum of the strap and lap thickness equals two times the strap thickness t , the equations could be simplified as follows:

$$\Delta G = \frac{(\Delta P)^2}{4b^2 Et} \quad (5)$$

Thus, the contribution of the adhesive stiffness is neglected since the adhesive is rather flexible and thin compared to the adherend parts. It should be pointed out, that bending effects due to

load eccentricity are ignored in this analysis. The Young's modulus E is derived by the use of strain gauges and amounts to 60.45 GPa for the quasi-isotropic stacking sequence that is used (see section 3).

6. DISCUSSION

As shown in Table 3, the measured maximum shear angle increases in a non-linear manner with the load level. It is assumed that the adhesive already shows plastic deformation to a certain extent for the highest load level. This assumption is also supported by the non-linear increase of the crack growth rate da/dN as shown in Table 3. However, the appearance of plastic deformation cannot be proven since the material's shear stress versus shear strain behavior is not available. This material data is going to be determined in following studies in tube torsion tests. The calculation of ΔG according to equation 5 is only valid for linear elastic deformations. Thus, a possible plastic share of the total adhesive deformation may lead to an error in the obtained ERR values. An evaluation of this error could be made by the use of a non-linear finite element analysis taking plasticity into account.

The independence of the crack growth from the actual crack length as discussed in section 2 is proven true by the predominant linear course of the crack length versus cycle number graphs in Fig. 7. The energy release rate is also independent of the crack length as shown in equation 5. Thus, the test setup is suitable for investigation of the crack growth as well as the determination of *Paris Law* data that is needed for fatigue simulation of bonded joints based on fracture mechanic approaches, for instance cohesive zone modeling (CZM).

By the use of the zigzag shaped release film, an estimation of the crack growth threshold load level could be made as discussed in section 5. The value that is obtained using this method showed a very slow crack growth in the tests and is therefore very close to the assumed threshold. Thus, the method of increasing the bonded area in a linear manner by the use of release film could be a way for determination of the threshold value for other configurations or other material systems as well.

Table 3. Averaged crack growth rate da/dN [$\mu m/cycle$] and corresponding measured maximum shear angle [γ] within the adhesive for several load levels

F_{max} [kN]	strap strain [$\mu m/m$]	da/dN [$\mu m/cycle$]	shear angle γ [$^\circ$]
5.16	1700	-	1.86
7.69	2500	0.018	2.56
9.28	3000	0.119	3.14
10.85	3500	0.335	3.82
12.43	4000	0.687	4.60
15.60	5000	4.157	6.49

7. CONCLUSION

The CLS test is a suitable configuration for fatigue crack growth studies of bonded joints, since it represents a realistic shear dominant loading case and allows stable and linear crack propagation. The results are therefore useful to obtain material data as input for fatigue models. Moreover, the CLS test is applicable for examinations of crack-constraining design features. Further experimental work will focus on evaluating the crack-stopping ability of several design features that are under investigation within the BOPACS project.

The strain measurements using high-resolution DIC turned out to be very useful to investigate the shear deformation of the adhesive along the bondline. The results give insight into the distribution of strain which is not feasible with other strain measurement systems and is therefore of high interest especially for comparison with simulation results.

8. ACKNOWLEDGEMENTS

The presented results are obtained within the project BOPACS of the Seventh Framework Program (FP7). The authors kindly acknowledge the European Commission for funding the research. Appreciations are extended to those who contributed to this work.

References

- [1] A. A. Baker, S. Dutton, K. Donald, *Composite materials for aircraft structures*. 2th ed. American Institute of Aeronautics and Astronautics, 2004.
- [2] T. Kruse, Bonding of CFRP Primary Aerospace Structures: Overview in the Technology Status in the Context of the Certification Boundary Conditions Addressing Needs for Development. In *19th International Conference on Composite Materials*, ICCM 19, 5635-5643, 2013.
- [3] D. N. Markatos, K. I. Tserpes, E. Rau, S. Markus, B. Erhardt, S. Pantelakis, The effects of manufacturing-induced and in-service related bonding quality reduction on the mode-I fracture toughness of composite bonded joints for aeronautical use. *Composites: Part B*, 45, 556-564, 2013.
- [4] U.S. Department of Transportation - Federal Aviation Administration (FAA). *AMC 20-29 Annex II to ED Decision 2010/003/R of 19/07/2010*. FAA , 2009.
- [5] European Aviation Safety Agency (EASA). *Advisory Circular 20-107B - Subject: Composite Aircraft Structure*. EASA, 2010.
- [6] J. Casas-Rodriguez, J. P. Ashcroft, V. V. Silberschmidt, Damage in adhesively bonded CFRP joints: Sinusoidal and impact-fatigue. *Composites Science and Technology*, 68(13), 2663-2670, 2008.

- [7] I. A. Ashcroft, M. M. Abdel, A. D. Crocombe, D. J. Hughes, S. J. Shaw, The effect of environment on the fatigue of bonded composite joints. Part 1: testing and fractography. *Composites Part A: Applied Science and Manufacturing*, 32(1), 45-58, 2001.
- [8] N. V. Datla, M. Papini, J. A. Schroeder, J. K. Spelt, Modified DCB and CLS specimens for mixed-mode fatigue testing of adhesively bonded thin sheets. *International Journal of Adhesion and Adhesives*, 30(6), 439-447, 2010.
- [9] D. Elder, B. Qi, High strain rate behavior of bonded composite joints. In: Camanho P, Tong L. *Composite joints and connections*. Cambridge: Woodhead Publishing; 2011, p. 484-507.
- [10] J. Tomblin, K. Strole, G. Dodosh, L. Ilcewitz, *Assessment of Industry Practices for Aircraft Bonded joints and Structures*. FAA Report DOT/FAA/AR-05/13, Washington, 2005.
- [11] W. S. Johnson, *Stress Analysis of the Crack Lap Shear Specimen. An ASTM Round Robin*. NASA Technical Memorandum 89006, 1986.
- [12] C. H. Wang, *Introduction to fracture mechanics*. DSTO-GD-0103. Aeronautical and Maritime Research Laboratory, 1996.
- [13] K. Y. Lin, W. Liu, Delamination Arrest of Fasteners in Aircraft Composite Structures. In *19th International Conference on Composite Materials, ICCM 19*, 1577-1580, 2013.